

Effects of Cavity and Superradiance on the Electrical Transport Through Quantum Dots

Y.N. Chen¹, D.S. Chuu¹ and T. Brandes²

¹Department of Electrophysics, National Chiao-Tung University, Hsinchu 300, Taiwan

²Department of Physics, UMIST, P.O. Box 88, Manchester, M60 1QD, U.K.

Abstract

A novel method is proposed to measure the Purcell effect by observing the current through a semiconductor quantum dot embedded inside a microcavity. The stationary current is shown to be altered if one varies the cavity length. For the double-dot system, the stationary current is found to show the interference feature (superradiance) as the inter-dot distance is varied. The amplitude of oscillation can be increased by incorporating the system into a microcavity. Furthermore, the current is suppressed if the dot distance is small compared to the wavelength of the emitted photon. This photon trapping phenomenon generates the entangled state and may be used to control the emission of single photons at predetermined times.

1 Introduction

Since Dicke proposed the idea of superradiance[1], coherent radiation phenomena for atomic systems was intensively investigated[2, 3, 4, 5, 6]. What Dicke found was that when the gas is in a particular state with the half number of molecules excited, the spontaneous emission rate of the whole gas is proportional to the square of the molecular concentration, provided that the gas volume dimension is small compared to the emitted photon wavelength. One of the interests in superradiant study lies in its close connection with the physics of laser emission. In some aspect, the superradiant phenomena appears somewhat simpler since one can neglect the pumping and relaxation mechanisms which are important in laser operation and consider only the evolution of atoms exclusively coupled to their own radiation field.

In solid state physics, the exciton-polariton state is one of the limiting cases of superradiance. When a Frenkel exciton couples to the radiation field in a small system which contains N lattice points, it represents one excited atom and $N - 1$ unexcited atoms in the others. According to Dicke's theory, the decay rate of the system will be

enhanced by a factor N . But as it was well known in a 3-D bulk crystal[7], the exciton will couple with photon to form polariton—the eigenstate of the combined system consisting of the crystal and the radiation field which does not decay radiatively. What makes the exciton trapped in the bulk crystal is the conservation of crystal momentum. If one considers a linear chain or a thin film, the radiative recombination of excitons is fundamentally different from the three-dimensional case. In bulk crystal, radiative decay requires phonons or other translational-invariance breaking entities such as defects, impurities, or interfaces. Thin films or linear chains, however, inherently break translational invariance. As a consequence, a radiative decay channel opens up, and the decay rate of the exciton is enhanced by a factor of λ/d in a linear chain[8] and $(\lambda/d)^2$ for 2D exciton-polariton[9, 10], where λ is the wave length of emitted photon and d is the lattice constant of the linear chain or the thin film.

With the advances of microfabrication technologies such as molecular beam epitaxy, it has become possible to fabricate various structures of microcrystals with fine quality and novel properties, such as quantum well, superlattice, quantum dot, quantum wire, and quantum ring. The exciton in a quantum well can exhibit the behavior between purely three dimensions and two dimensions. Many investigations on the radiative linewidth of excitons in quantum wells have been performed [11, 12, 13, 14, 15, 16, 17]. For lower dimensional systems, first observation of superradiant short lifetimes of excitons was performed by Ya. Aaviksoo *et al.*[18] on surface states of the anthracene crystal. Superradiance has also been discussed for one-dimensional (1D) Frenkel excitons in disordered aggregates.[19, 20] A. L. Ivanov and H. Haug[21] predicted the existence of exciton crystal, which favors coherent emission in the form of superradiance, in quantum wires. Y. Manabe *et al.*[22] considered the superradiance of interacting Frenkel excitons in a linear chain. For quantum dots of CuCl with radii R between 18 and 77 Å, the superradiance of excitons was also observed by Nakamura *et al.*[23]. The decay rate was shown to be proportional to $R^{2.1}$ which confirms the theoretical prediction by Hanamura.[13] Similar works were also obtained by Itch *et al.*[24]. By using numerical simulation, Spano *et al.* [24] have also showed the effective coherent size (which is inversely proportional to the decay time in their definition) decreases as the temperature increases. Recently, superradiance of polaritons from a dimer to finite one-dimensional crystal has also been discussed by Dubovskii.[26]

In reality, superradiance is accompanied by frequency shift, as pointed by Lee *et al.*[27]. However, the coherent frequency shift of an exciton has received fewer attention. One of the reasons is the difficulty arose from the divergent nature of frequency shift, both infrared and ultraviolet. Lee *et al.* [28] have solved the problem by using the method of renormalization for a system of two atoms, and applied to the case of excitons in a thin semiconductor film.[27] Recently, we have generalized their results to the quantum well systems.[29] The crossover behavior from 2D film to 3D crystal was also examined. It was found that both the decay rate and renormalized

frequency shift show oscillatory dependence on layer thickness.

On the other hand, Purcell[30] predicted that the spontaneous emission rate, and thus the relaxation lifetime of an excited atom, would be altered if the atom was put in a cavity with dimensions comparable to the transition wavelength of the atom. The reason for modified spontaneous emission rate is that spontaneous emission can be viewed as stimulated emission, stimulated by vacuum-field fluctuations. Hence, the lifetime can be altered by modifying the photon density of states.

In the last few years, experiments which have confined photons in low-dimensional semiconductor quantum structures by using optical microcavities were in progress. Research on combined quantum confined 2D carriers and 2D photon states has been performed by using quantum wells embedded in planar microcavities, yielding interesting physics both in the weak and strong carrier-photon coupling regimes.[31] Results from 2D carriers combined with 1D (0D) photon states have also been studied [32, 33]. Introducing further degrees of carrier confinement in such microcavity structures is a natural trend in this field. Recently, the incorporation of quantum dots in planar and pillar microcavities have been reported.[34] A coupling between 1D electron state and 2D photon states were also obtained by inserting an array of quantum wires into a planar microcavity.[35] Such systems lead to dramatic changes in the exciton-polariton dispersion[36] and exciton lifetime.[37, 38]

In this manuscript, an alternative way is proposed to observe the inhibited or enhanced spontaneous emission by embedding a quantum dot inside a microcavity[21]. After the injection of an electron and hole into a quantum dot, a photon is generated by the recombination of the exciton. This process allows one to determine Purcell effect by measuring the current through the quantum dot. Similarly, by embedding two quantum dots inside the cavity and controlling the gate voltage of one of the dots, one can not only determine the superradiant effect by measuring the stationary current, but also induces the entangled states, which is one of the fundamental requirements for quantum information processing .

This paper is organized as follows. A brief description of superradiant and Purcell effects is reviewed in section II. In section III, we discussed the transport properties of a two level quantum dot embedded in a planar microcavity. Electrical measurements of superradiance and the generated entanglement are shown in section IV. Finally, overall conclusions are presented in the last section.

2 A brief review of Superradiant and Purcell effect

2.1 Spontaneous emission of two coupled atoms

Spontaneous emission is one of the fundamental concepts in quantum mechanics that can be traced back to the early works of Albert Einstein.[39] In free space a two level atom interacts with a continuum of radiation field modes, which leads to an irreversible exponential decay of the excitation. In this subsection, the

Weisskopf-Wigner theory of spontaneous emission for two level atoms in free space is reviewed.[40]

The total Hamiltonian for a single two level atom in the rotating wave approximation (RWA) is given by

$$H = \frac{1}{2}\hbar\omega\hat{\sigma}_z + \sum_{\mathbf{q}} \hbar\omega_{\mathbf{q}}(b_{\mathbf{q}}^{\dagger}b_{\mathbf{q}} + \frac{1}{2}) - \sum_{\mathbf{q}} \hbar D_{\mathbf{q}}(b_{\mathbf{q}}^{\dagger}\hat{\sigma}_- + b_{\mathbf{q}}\hat{\sigma}_+), \quad (2.1)$$

where $\hat{\sigma}_z = |\uparrow\rangle\langle\uparrow| - |\downarrow\rangle\langle\downarrow|$ and $\hat{\sigma}_+ = |\uparrow\rangle\langle\downarrow|$, $\hat{\sigma}_- = |\downarrow\rangle\langle\uparrow|$ are the Pauli matrices in the 2×2 space, $\hbar\omega$ is the level spacing between the two levels, and $D_{\mathbf{q}} = (\frac{\omega_{\mathbf{q}}}{2\epsilon_0\hbar V})^{1/2} \vec{\epsilon} \cdot \vec{\mu}$ is the dipole coupling matrix element. Furthermore, $\omega_{\mathbf{q}} = c|\mathbf{q}|$, and $b_{\mathbf{q}}^{\dagger}$ creates a photon with wave vector \mathbf{q} .

In the interaction picture, the combined atom-field system is represented by

$$|\psi(t)\rangle = f_0(t)|\uparrow; 0\rangle + \sum_{\mathbf{q}} f_{G;\mathbf{q}}(t)|\downarrow; 1_{\mathbf{q}}\rangle, \quad (2.2)$$

where $|\downarrow; 1_{\mathbf{q}}\rangle$ represents the state in which the atom is in the ground state and the field mode \mathbf{q} has one photon.

Substituting Eq. (2.1) into Schrödinger equation and projecting into each state, we obtain

$$f_0(t) = \exp[-(\frac{1}{2}\Gamma + i\Delta\omega)t], \quad (2.3)$$

where

$$\begin{aligned} \Gamma &= \frac{1}{3\pi\epsilon_0\hbar c^3} \int d\omega_{\mathbf{q}} \omega_{\mathbf{q}}^3 \mu^2 \delta(\omega - \omega_{\mathbf{q}}) \\ &= \frac{\omega^3 \mu^2}{3\pi\epsilon_0\hbar c^3}, \end{aligned} \quad (2.4)$$

and

$$\Delta\omega = \frac{1}{6\pi^2} \epsilon_0 \hbar c^3 \mathcal{P} \int d\omega_{\mathbf{q}} \frac{\omega_{\mathbf{q}}^3 \mu^2}{\omega - \omega_{\mathbf{q}}}. \quad (2.5)$$

The spontaneous decay rate Γ gives the Einstein's A coefficient, and the frequency shift $\Delta\omega$ represents the Lamb shift.[41]

In a system of *two identical atoms* interacting via common radiation field, the decay splits into a sub- and a superradiant channel. The Hamiltonian for two atoms interacting with the electromagnetic field reads

$$\begin{aligned}
H &= H_0 + H_{ph} + H_{eph} \\
H_0 &= \frac{1}{2}\hbar\omega(\hat{\sigma}_{1,z} + \hat{\sigma}_{2,z}) \\
H_{ph} &= \sum_{\mathbf{q}} \hbar\omega_{\mathbf{q}}(b_{\mathbf{q}}^\dagger b_{\mathbf{q}} + \frac{1}{2}) \\
H_{eph} &= \sum_{j=1,2} \hbar D_{\mathbf{q}}(b_{\mathbf{q}}^\dagger e^{i\mathbf{q}\cdot\mathbf{r}_j} \hat{\sigma}_{j,-} + b_{\mathbf{q}} e^{-i\mathbf{q}\cdot\mathbf{r}_j} \hat{\sigma}_{j,+}), \tag{2.6}
\end{aligned}$$

where $\hat{\sigma}_{j,-}$, $\hat{\sigma}_{j,+}$ and $\hat{\sigma}_{j,z}$ are the Pauli matrices in the 2×2 space of the upper/lower level $|\uparrow\rangle^j, |\downarrow\rangle^j$ of atom j , $\hbar\omega$ is the level spacing between the two level, and $D_{\mathbf{q}} = (\frac{\omega_{\mathbf{q}}}{2\epsilon_0\hbar V})^{1/2} \vec{e} \cdot \vec{\mu}$ is the dipole coupling matrix element. Furthermore, $\omega_{\mathbf{q}} = c|\mathbf{q}|$, and $b_{\mathbf{q}}^\dagger$ creates a photon with wave vector \mathbf{q} .

One can define the so-called Dicke state,

$$\begin{aligned}
|S_0\rangle &= \frac{1}{\sqrt{2}}(|\uparrow\downarrow\rangle - |\downarrow\uparrow\rangle) \\
|T_1\rangle &= |\uparrow\uparrow\rangle \\
|T_0\rangle &= \frac{1}{\sqrt{2}}(|\uparrow\downarrow\rangle + |\downarrow\uparrow\rangle) \\
|T_{-1}\rangle &= |\downarrow\downarrow\rangle. \tag{2.7}
\end{aligned}$$

Using this basis, one can easily calculate the matrix elements

$$\begin{aligned}
\langle T_1 | \hat{\sigma}_{j,\pm} | T_1 \rangle &= \langle T_1 | \hat{\sigma}_{j,\pm} | T_{-1} \rangle = 0, \quad j = 1, 2 \\
\langle T_1 | \hat{\sigma}_{j,+} | T_0 \rangle &= \langle T_0 | \hat{\sigma}_{j,+} | T_{-1} \rangle = \frac{1}{\sqrt{2}}, \quad j = 1, 2 \\
\langle T_0 | \hat{\sigma}_{j,\pm} | S_0 \rangle &= 0, \quad j = 1, 2 \\
\langle T_1 | \hat{\sigma}_{1,+} | S_0 \rangle &= -\frac{1}{\sqrt{2}}, \quad \langle T_1 | \hat{\sigma}_{2,+} | S_0 \rangle = \frac{1}{\sqrt{2}} \\
\langle S_0 | \hat{\sigma}_{1,+} | T_{-1} \rangle &= \frac{1}{\sqrt{2}}, \quad \langle S_0 | \hat{\sigma}_{2,+} | T_{-1} \rangle = -\frac{1}{\sqrt{2}}. \tag{2.8}
\end{aligned}$$

This means that there are two transition rate Γ_{\pm} for spontaneous of photons into a vacuum state,

$$\Gamma_{\pm}(q) = 2\pi \sum_{\mathbf{q}} \frac{|\alpha_{\mathbf{q}} \pm \beta_{\mathbf{q}}|^2}{2} \delta(\omega - \omega_{\mathbf{q}}), \quad q = \frac{\omega}{c}, \tag{2.9}$$

where we have defined $\alpha_{\mathbf{q}} = D_{\mathbf{q}}e^{i\mathbf{q}\cdot\mathbf{r}_1}$ and $\beta_{\mathbf{q}} = D_{\mathbf{q}}e^{i\mathbf{q}\cdot\mathbf{r}_2}$. Evaluation of this expression yields

$$\Gamma_{\pm}(q) = \Gamma\left[1 \pm \frac{\sin(qd)}{qd}\right], \quad (2.10)$$

where $\Gamma \propto q^3$ is the decay rate of an isolated atom. Here, $d = |\mathbf{r}_1 - \mathbf{r}_2|$ is the distance between the two atoms. The appearance of two decay channels has been discovered by Dicke [1] and observed by DeVoe and Brewer[42] in a laser-trapped two-ion system.

The time-dependence of the collective decay of two radiators is different from the decay of two single radiators. If we denote the occupation probabilities of the four levels by $T_1(t)$, $T_0(t)$, $T_{-1}(t)$, and $S_0(t)$, the time dependence occupations is then governed by two decay rates Γ_+ and Γ_- :

$$\begin{aligned} \dot{T}_1 &= -(\Gamma_+ + \Gamma_-)T_1 \\ \dot{S}_0 &= \Gamma_-(T_1 - S_0) \\ \dot{T}_0 &= \Gamma_+(T_1 - T_0) \\ \dot{T}_{-1} &= \Gamma_+T_0 + \Gamma_-S_0. \end{aligned} \quad (2.11)$$

The above equation can be solved easily,

$$\begin{aligned} T_1(t) &= e^{-(\Gamma_+ + \Gamma_-)t} \\ S_0(t) &= \frac{[e^{-\Gamma_-t} - e^{-(\Gamma_- + \Gamma_+)t}]\Gamma_-}{\Gamma_+} \\ T_0(t) &= \frac{[e^{-\Gamma_+t} - e^{-(\Gamma_- + \Gamma_+)t}]\Gamma_+}{\Gamma_-} \\ T_{-1}(t) &= \frac{\Gamma_- \Gamma_+ - e^{-(\Gamma_- + \Gamma_+)t} [(-1 + e^{\Gamma_+t})\Gamma_-^2 + \Gamma_- \Gamma_+ + (-1 + e^{\Gamma_-t})\Gamma_+^2]}{\Gamma_- \Gamma_+}, \end{aligned} \quad (2.12)$$

where initial conditions $T_1(0) = 1$, $S_0(0) = T_0(0) = T_{-1}(0) = 0$ have been assumed. If we consider the special case where $\Gamma_- = 0$ and $\Gamma_+ = 2\Gamma$, this would correspond to the case $qd \rightarrow 0$, i.e. the wavelength of the emitted photon is much larger than the distance between the two radiators. Then, Eq. (2.12) reduced to

$$\begin{aligned} T_1(t) &= e^{-\Gamma_+t} \\ T_0(t) &= \Gamma_+ t e^{-\Gamma_+t} \\ S_0(t) &= 0 \\ T_{-1}(t) &= 1 - e^{-\Gamma_+t}(1 + \Gamma_+t). \end{aligned} \quad (2.13)$$

The total coherent emission rate $I_2(t)$ at time t is the sum of the emission rates from T_1 and T_0 :

$$I_2(t) = E_0\Gamma_+e^{-\Gamma_+t}(1 + \Gamma_+t), \quad \Gamma_+ = 2\Gamma, \quad (2.14)$$

where E_0 is a constant with dimension energy. This is different to the incoherent sum $2I_1(t)$ of the emission rates $I_1(t)$ from two independent radiators, which would give

$$2I_1(t) = 2E_0\Gamma e^{-\Gamma t}. \quad (2.15)$$

2.2 Effect of cavity on the radiative decay of excitons in low dimensional systems

As we mentioned above, the electron-hole pair is naturally a candidate for examining spontaneous emission and Purcell effect. Let us first consider a Wannier exciton in a quantum ring with radius $\rho \sim Nd/2\pi$, where d is the lattice spacing and N is the number of the lattice points. In our model, the circular ring is joined by the N lattice points, and we also assume the effective mass approximation is valid in the circumference direction. The state of the Wannier exciton can be specified as $|\nu, n, m\rangle$, where ν is the exciton wave number. n and m are quantum numbers for internal structure of the exciton, and will be specified later. Here, ν takes the value of an integer. The matter Hamiltonian can be written as

$$H_{ex} = \sum_{\nu nm} E_{\nu nm} c_{\nu nm}^\dagger c_{\nu nm}, \quad (2.16)$$

where $c_{\nu nm}^\dagger$ and $c_{\nu nm}$ are the creation and destruction operators of the exciton, respectively. The Hamiltonian of free photon is

$$H_{ph} = \sum_{\mathbf{q}'k'_z} \hbar c (q'^2 + k_z'^2)^{1/2} b_{\mathbf{q}'k'_z\lambda}^\dagger b_{\mathbf{q}'k'_z\lambda}, \quad (2.17)$$

where $b_{\mathbf{q}'k'_z\lambda}^\dagger$ and $b_{\mathbf{q}'k'_z\lambda}$ are the creation and destruction operators of the photon, respectively. The wave vector \mathbf{k}' of the photon is separated into two parts: k'_z is the perpendicular component of \mathbf{k}' on the ring plane such that $k'^2 = q'^2 + k_z'^2$.

The interaction between the exciton and the photon can be expressed as

$$H' = \sum_{k'_z nm} \sum_{\mathbf{q}'} D_{\mathbf{q}'k'_z\nu nm} b_{k'_z\mathbf{q}'}^\dagger c_{\nu nm}^\dagger + \text{h.c.}, \quad (2.18)$$

where

$$D_{\mathbf{q}'k'_z\nu nm} = H_\nu^{(1)}(q'\rho) \frac{e}{mc} \sqrt{\frac{2\pi\hbar c}{(q'^2 + k_z'^2)^{1/2} v}} \epsilon_{\mathbf{q}'k'_z} A_{\nu nm} \quad (2.19)$$

with $\epsilon_{\mathbf{q}'k'_z}$ being the polarization of the photon and $H_\nu^{(1)}$ is the Hankel function. In Eq. (2.19),

$$A_{\nu nm} = \sqrt{N} \sum_{\varphi_e} F_{nm}(\varphi_e) \int d\varphi w_c(\varphi - \varphi_e) \times \exp(i\nu(\varphi - \frac{m_e^* \varphi_e}{m_e^* + m_h^*})) (-i\hbar \frac{\partial}{\partial \varphi}) w_\nu(\varphi). \quad (2.20)$$

is the effective transition dipole matrix element and $F_{nm}(\varphi_e)$ is the hydrogenic wavefunction in the ring. Here, m_e^* and m_h^* are, respectively, the effective masses of the electron and hole.

The decay rate of the exciton can be expressed as

$$\gamma_{\nu nm} = 2\pi \sum_{\mathbf{q}'k'_z\lambda} |D_{\mathbf{q}'k'_z\nu nm}|^2 \delta(\omega_{\mathbf{q}'k'_z\nu nm}), \quad (2.21)$$

where $\omega_{\mathbf{q}'k'_z\nu nm} = E_{\nu nm}/\hbar - c\sqrt{q'^2 + k_z'^2}$. The Wannier exciton decay rate in the optical region can be calculated straightforwardly and is given by

$$\gamma_{\nu nm} = \frac{e^2 \hbar \rho}{m^2 c d} \int |H_\nu^{(1)}(q'\rho)|^2 q' \int \frac{\delta(\omega_{\mathbf{q}'k'_z\nu nm})}{\sqrt{k_z'^2 + q'^2}} |\epsilon_{\mathbf{q}'k'_z\lambda} \cdot \chi_{\nu nm}|^2 dk'_z dq', \quad (2.22)$$

where

$$\chi_{\nu nm} = \sum_{\varphi_e} F_{nm}^*(\varphi_e) \int d\varphi w_c^*(\varphi - \varphi_e) (-i\hbar \frac{\partial}{\partial \varphi}) w_\nu(\varphi). \quad (2.23)$$

From Eq. (2.22), one observes that the decay rate $\gamma_{\nu nm}$ is proportional to ρ/d . This is just the superradiance factor coming from the coherent contributions of atoms within half a wavelength or so. In Fig. 1 we have numerically calculated the superradiant decay rate in $\nu = 0, n = 0$, and $m = 0$ mode. In plotting the figure, we have assumed $E_{\nu nm}/\hbar = k_0 = 2\pi/\lambda$, $\lambda = 8000\text{\AA}$, $d = 5\text{\AA}$, γ_0 is the decay rate of an isolated atom, and for large radius, F_{nm}^* is independent of ρ . The decay rate increases linearly with the increasing of radius when the radius is small. This linear regime agrees with Dicke's prediction: For one excited atom and $N - 1$ unexcited atoms in a small volume, the decay rate is enhanced by the factor of $1 \times N$. For large radius, the decay rate can approach 1D limit ($= \frac{3\pi}{2k_0 d} \gamma_0$) correctly.

Quite recently, R. A. Römer and M. E. Raikh studied theoretically the exciton absorption shredded by a magnetic flux Φ [43]. From their results, effects of magnetic flux on exciton wavefunction F_{nm}^* can not be neglected in small radius limit, and may be examined from the variations of the decay rate. In the inset of Fig. 1, three curves of different flux Φ are presented as functions of radius ρ . The dashed, solid,

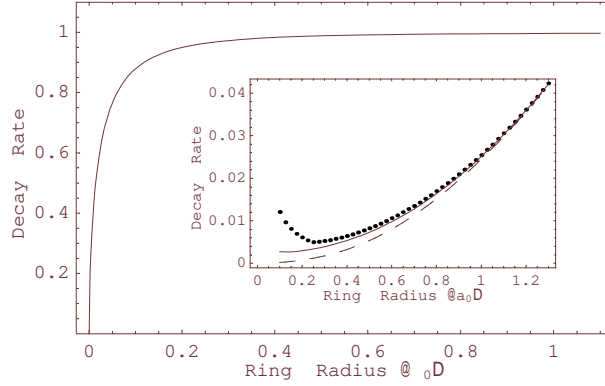


Figure 1: Decay rate of a quantum ring exciton in large radius limit, i.e. F_{nm}^* are assumed to be independent of ρ . The vertical unit and horizontal units are $\frac{3\pi}{2k_0d}\gamma_0$ and λ_0 , respectively. Inset : Effect of Aharonov-Bohm on the radiative decay of quantum ring exciton. The dashed(— —), solid, and dashed-dotted(— ·) curves correspond to $\Phi = 0\Phi_0$, $0.25\Phi_0$, and $0.5\Phi_0$, respectively. In small radius limit, F_{nm}^* depends strongly on radius ρ , and its influence on the decay rate is evident. The vertical and horizontal units here are $\frac{3\pi}{2k_0d}\gamma_0$ and ring radius (in units of a_0), respectively.

and dotted curves represent the cases of $\Phi = 0\Phi_0$, $0.25\Phi_0$, and $0.5\Phi_0$, respectively. For $\Phi = 0.5\Phi_0$, the decay rate decreases as the ring radius becomes small but reaches the minimum point as ρ is about $0.25a_0$ (where a_0 is the effective Bohr radius we assumed in 1D limit). This is because the probability, for electron and hole to meet each other on the opposite side of the ring, increases with the decreasing of ring radius, while the coherent effect decreases with the decreasing of the radius. Therefore, there is a competition between these two effects as one decreases the radius. In Fig. 2, relative decay rate $[\gamma_{\nu nm}(\Phi) - \gamma_{\nu nm}(\Phi = 0)]$ is plotted as a function of magnetic flux Φ with different radius. The solid and dashed lines represent the cases of $\rho = 1 a_0$ and $\rho = 0.5 a_0$, respectively. As expected, the larger the radius, the smaller the AB oscillation amplitude. Besides, the superradiant decay rate is most enhanced for $\Phi = 0.5\Phi_0$, and the oscillation period is equal to $\Phi_0 = hc/e$.

We now consider a Wannier exciton in a quantum ring embedded in perfectly reflecting mirrors with cavity length L_c . The decay rate of the quantum ring exciton can be expressed as

$$\gamma_\nu = \sum_{n_c} \frac{e^2 \hbar}{m^2 c^2 L_c d} \frac{\rho}{d} \left| H_\nu^{(1)}(\sqrt{(2\pi/\lambda)^2 - (\pi n_c/L_c)^2} \rho) \right|^2 |\epsilon_{\mathbf{q}'k'_z} \cdot \chi_\nu|^2. \quad (2.24)$$

The numerical calculations of Eq. (2.24) are shown in the left panel of Fig. 3. As can be seen, the decay rate of a quantum ring exciton shows the enhanced peaks as the cavity length L_c is equal to multiple half-wavelengths of the emitted photon.

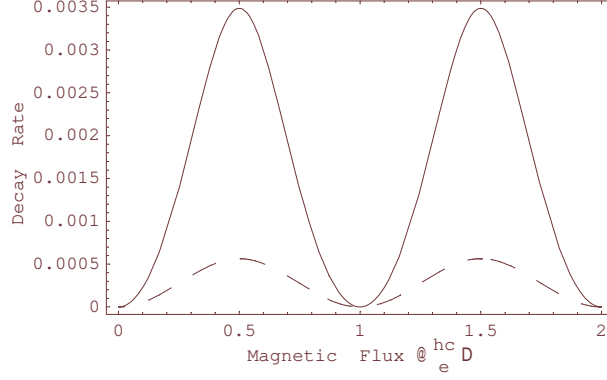


Figure 2: Dependence of relative decay rate $[\gamma_{\nu nm}(\Phi) - \gamma_{\nu nm}(\Phi = 0)]$ on the magnetic flux. The dashed and solid curves correspond to $\rho = 0.5 a_0$ and $\rho = 1 a_0$, respectively. The vertical and horizontal units are $\frac{3\pi}{2k_0 d} \gamma_0$ and universal flux quantum $\Phi_0 = hc/e$, respectively.

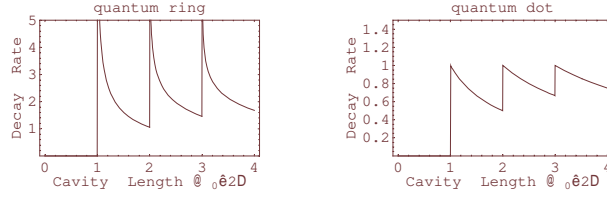


Figure 3: Left panel : Decay rate of a quantum ring exciton in a planar microcavity with radius $\rho = \lambda/2\pi$. The horizontal and vertical units are $(\lambda/2)$ and $\frac{e^2 \hbar \lambda^2}{4\pi^3 m^2 c^2 d} |\epsilon_{\mathbf{q}' k'_z} \cdot \chi_\nu|^2$, respectively. Right Panel : Similar case for a quantum dot exciton.

However, if one considers a quantum dot exciton inside the microcavity, the decay rate reads

$$\gamma \propto \sum_{n_c} \frac{e^2 \hbar}{m^2 c^2 L_c} \theta((2\pi/\lambda)^2 - (\pi n_c/L_c)^2) |\epsilon_{\mathbf{q}' k'_z} \cdot \chi|^2, \quad (2.25)$$

where θ is the step function. The numerical calculations are presented in the right panel of Fig. 3. One can see from the figure, there is no enhanced peak with the increasing of the cavity length. This is because the angular momentum (translational momentum) of the exciton in a quantum ring is conserved in circular direction, while the crystal symmetry is totally broken in a quantum dot. Due to the modification of the density of states of the photon in the microcavity, the decay rate of the exciton shows enhanced peaks in 1D systems[38] and zigzag structure in 0D quantum dot. One also notes that such kind of peak maybe a useful feature to realize the Aharonov-Bohm effect for an exciton in a quantum ring. Generally speaking, the

excitonic AB oscillation is very small and hard to be measured. However, if one can incorporate the quantum ring inside the planar microcavities, the AB oscillation may be enhanced at these peaks.

3 Current through one quantum dot and Purcell effect

We now consider a quantum dot embedded in a $p-i-n$ junction which is similar to the device proposed by O. Benson *et al*[44]. The energy-band diagram is shown in Fig. 4.

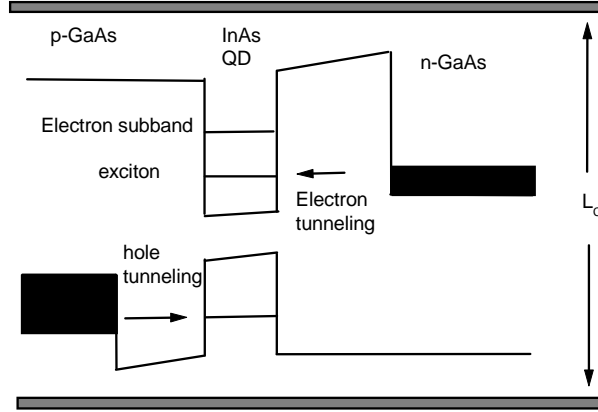


Figure 4: Energy-band diagram of the p-i-n junction.

Both the hole and electron reservoirs are assumed to be in thermal equilibrium. For the physical phenomena we are interested in, the fermi level of the $p(n)$ -side hole (electron) is slightly lower (higher) than the hole (electron) subband in the dot. After a hole is injected into the hole subband in the quantum dot, the n -side electron can tunnel into the exciton level because of the Coulomb interaction between the electron and hole. Thus, we may assume three dot states

$$\begin{aligned}
 |0\rangle &= |0, h\rangle \\
 |U\rangle &= |e, h\rangle \\
 |D\rangle &= |0, 0\rangle
 \end{aligned} \tag{3.1}$$

, where $|0, h\rangle$ means there is one hole in the quantum dot, $|e, h\rangle$ is the exciton state, and $|0, 0\rangle$ represents the ground state with no hole and electron in the quantum dot. One might argue that one can not neglect the state $|e, 0\rangle$ for real device since the tunable variable is the applied voltage. This can be resolved by fabricating a thicker barrier on the electron side so that the probability for an electron to tunnel in advance is very small. Moreover, the charged exciton and biexcitons states are

also neglected in our calculations. This means a low injection limit is required in the experiment[45]. We can now define the dot-operators $\hat{n}_U \equiv |U\rangle \langle U|$, $\hat{n}_D \equiv |D\rangle \langle D|$, $\hat{p} \equiv |U\rangle \langle D|$, $\hat{s}_U \equiv |0\rangle \langle U|$, $\hat{s}_D \equiv |0\rangle \langle D|$. The total hamiltonian H of the system consists of three parts: the dot hamiltonian, the photon bath, and the electron (hole) reservoirs:

$$\begin{aligned}
H &= H_0 + H_T + H_V \\
H_0 &= \varepsilon_U \hat{n}_U + \varepsilon_D \hat{n}_D + H_p + H_{res} \\
H_T &= \sum_k g(D_k b_k^\dagger \hat{p} + D_k^* b_k \hat{p}^\dagger) = g(\hat{p} X + \hat{p}^\dagger X^\dagger) \\
H_p &= \sum_k \omega_k b_k^\dagger b_k \\
H_V &= \sum_{\mathbf{q}} (V_{\mathbf{q}} c_{\mathbf{q}}^\dagger \hat{s}_U + W_{\mathbf{q}} d_{\mathbf{q}}^\dagger \hat{s}_D + c.c.) \\
H_{res} &= \sum_{\mathbf{q}} \varepsilon_{\mathbf{q}}^U c_{\mathbf{q}}^\dagger c_{\mathbf{q}} + \sum_{\mathbf{q}} \varepsilon_{\mathbf{q}}^D d_{\mathbf{q}}^\dagger d_{\mathbf{q}}.
\end{aligned} \tag{3.2}$$

In above equations, b_k is the photon operator, gD_k is the dipole coupling strength, $X = \sum_k D_k b_k^\dagger$, and $c_{\mathbf{q}}$ and $d_{\mathbf{q}}$ denote the electron operators in the left and right reservoirs, respectively. Here, g is a constant with a unit of the tunneling rate. The couplings to the electron and hole reservoirs are given by the standard tunnel hamiltonian H_V , where $V_{\mathbf{q}}$ and $W_{\mathbf{q}}$ couple the channels \mathbf{q} of the electron and the hole reservoirs. If the couplings to the electron and the hole reservoirs are weak, then it is reasonable to assume that the standard Born-Markov approximation with respect to these couplings is valid. In this case, we will derive a master equation from the exact time-evolution of the system.

In interaction picture, time evolutions of arbitrary operators \hat{O} and X are defined by

$$\tilde{O}(t) \equiv e^{iH_0 t} O e^{-iH_0 t}, \quad X_t \equiv e^{iH_0 t} X e^{-iH_0 t}. \tag{3.3}$$

Furthermore, for the total density matrix $\Xi(t)$ which obeys the Liouville equation

$$\Xi(t) = e^{-iHt} \Xi_{t=0} e^{iHt}, \tag{3.4}$$

and we also define

$$\tilde{\Xi}(t) \equiv e^{iH_0 t} \Xi(t) e^{-iH_0 t}. \tag{3.5}$$

The expectation value of any operator \hat{O} is given by

$$\langle \hat{O} \rangle_t \equiv Tr(\Xi(t) O) = Tr(\tilde{\Xi}(t) \tilde{O}(t)). \tag{3.6}$$

We therefore have

$$\begin{aligned}
\widetilde{n}_U(t) &= \widehat{n}_U, \quad \widetilde{n}_D(t) = \widehat{n}_D \\
\widetilde{p}(t) &= \widehat{p} e^{i\epsilon t} X_t, \quad \widetilde{p}^\dagger(t) = \widehat{p}^\dagger e^{-i\epsilon t} X_t^\dagger \\
\varepsilon &\equiv \varepsilon_U - \varepsilon_D.
\end{aligned} \tag{3.7}$$

The equation of motion for $\widetilde{\Xi}(t)$ becomes

$$i \frac{d}{dt} \widetilde{\Xi}(t) = [\widetilde{H}_T(t) + \widetilde{H}_V(t), \widetilde{\Xi}(t)]. \tag{3.8}$$

This can be written as

$$\begin{aligned}
\frac{d}{dt} \widetilde{\Xi}(t) &= -i[\widetilde{H}_T(t), \widetilde{\Xi}(t)] - i[\widetilde{H}_V(t), \widetilde{\Xi}(t)] \\
&= -i[\widetilde{H}_T(t), \widetilde{\Xi}(t)] - i[\widetilde{H}_V(t), \Xi_0] \\
&\quad - \int_0^t dt' [\widetilde{H}_V(t), [\widetilde{H}_T(t'), \widetilde{H}_V(t'), \widetilde{\Xi}(t')]].
\end{aligned} \tag{3.9}$$

Now, we define the effective density operator of the dot plus photons,

$$\widetilde{\rho}(t) = \text{Tr}_{res} \widetilde{\Xi}(t) \tag{3.10}$$

as the trace of $\widetilde{\Xi}(t)$ over electron reservoirs. The trace Tr_{res} over the terms linear which are in H_V vanishes, therefore,

$$\frac{d}{dt} \widetilde{\rho}(t) = -i[\widetilde{H}_T(t), \widetilde{\rho}(t)] - \text{Tr}_{res} \int_0^t dt' [\widetilde{H}_V(t), [\widetilde{H}_V(t'), \widetilde{\Xi}(t')]]. \tag{3.11}$$

As can be seen from the above equation, the last term is already second order in H_V , we can approximate

$$\widetilde{\Xi}(t') \approx R_0 \widetilde{\rho}(t'), \tag{3.12}$$

where R_0 is the equilibrium density matrix for the two electron reservoirs. Working out the commutators and using the time evolution of the electron reservoir operators

$$\widetilde{c}_{\mathbf{q}}(t) = e^{-i\varepsilon_{\mathbf{q}}^L t} c_{\mathbf{q}}, \quad \widetilde{d}_{\mathbf{q}}(t) = e^{-i\varepsilon_{\mathbf{q}}^R t} d_{\mathbf{q}}, \tag{3.13}$$

the master equation becomes

$$\begin{aligned}
\tilde{\rho}(t) = & \rho_0 - i \int_0^t dt' [\widetilde{H}_T(t'), \tilde{\rho}(t')] \\
& - \Gamma_L \int_0^t dt' \{ \widetilde{s}_U(t') \widetilde{s}_U^\dagger(t') \tilde{\rho}(t') - 2 \widetilde{s}_U^\dagger(t') \tilde{\rho}(t') \widetilde{s}_U(t') \} \\
& - \Gamma_L \int_0^t dt' \{ \tilde{\rho}(t') \widetilde{s}_U(t') \widetilde{s}_U^\dagger(t') \} \\
& - \Gamma_R \int_0^t dt' \{ \widetilde{s}_D^\dagger(t') \widetilde{s}_D(t') \tilde{\rho}(t') \} \\
& - \Gamma_R \int_0^t dt' \{ -2 \widetilde{s}_D(t') \tilde{\rho}(t') \widetilde{s}_D^\dagger(t') + \tilde{\rho}(t') \widetilde{s}_D^\dagger(t') \widetilde{s}_D(t') \}, \tag{3.14}
\end{aligned}$$

where $\Gamma_L = \pi \sum_{\mathbf{q}} V_{\mathbf{q}}^2 \delta(\varepsilon_U - \varepsilon_{\mathbf{q}}^L)$ and $\Gamma_R = \pi \sum_{\mathbf{q}} W_{\mathbf{q}}^2 \delta(\varepsilon_D - \varepsilon_{\mathbf{q}}^R)$.

Multiplying Eq. (3.14) by \hat{n}_U , \hat{n}_D , \hat{p} , and \hat{p}^\dagger , respectively and performing the trace with the three dot states in Eq. (3.1), one obtains

$$\begin{aligned}
\langle \hat{n}_U \rangle_t - \langle \hat{n}_U \rangle_0 &= -ig \int_0^t dt' \{ \langle \hat{p} \rangle_{t'} - \langle \hat{p}^\dagger \rangle_{t'} \} + 2\Gamma_U \int_0^t dt' (1 - \langle \hat{n}_U \rangle_{t'} - \langle \hat{n}_D \rangle_{t'}) \\
\langle \hat{n}_D \rangle_t - \langle \hat{n}_D \rangle_0 &= -ig \int_0^t dt' \{ \langle \hat{p} \rangle_{t'} - \langle \hat{p}^\dagger \rangle_{t'} \} - 2\Gamma_D \int_0^t dt' \langle \hat{n}_D \rangle_{t'} \\
\langle \hat{p} \rangle_t - \langle \hat{p} \rangle_t^0 &= -\Gamma_D \int_0^t dt' e^{i\varepsilon(t-t')} \langle X_t X_{t'}^\dagger \tilde{p}(t') \rangle_{t'} \\
&\quad - ig \int_0^t dt' e^{i\varepsilon(t-t')} \{ \langle \hat{n}_U X_t X_{t'}^\dagger \rangle_{t'} - \langle \hat{n}_D X_t^\dagger X_{t'} \rangle_{t'} \} \\
\langle \hat{p}^\dagger \rangle_t - \langle \hat{p}^\dagger \rangle_t^0 &= -\Gamma_D \int_0^t dt' e^{-i\varepsilon(t-t')} \langle \tilde{p}^\dagger(t') X_{t'} X_t^\dagger \rangle_{t'} \\
&\quad + ig \int_0^t dt' e^{-i\varepsilon(t-t')} \{ \langle \hat{n}_U X_{t'} X_t^\dagger \rangle_{t'} - \langle \hat{n}_D X_t^\dagger X_{t'} \rangle_{t'} \}, \tag{3.15}
\end{aligned}$$

where $\varepsilon = \varepsilon_U - \varepsilon_D$ is the energy gap of the quantum dot exciton. Here, $\tilde{p}(t') = p e^{i\varepsilon t'} X_{t'}$, and $X_{t'}$ denotes the time evolution of X with H_p . The expectation value $\langle \hat{p}^{(\dagger)} \rangle_t^0$ describes the decay of an initial polarization of the system and plays no role for the stationary current. Therefore, we shall assume the initial expectation value of $\hat{p}^{(\dagger)}$ vanishes at time $t = 0$.

As can be seen from Eqs. (3.15), there are terms like $\langle \hat{n}_U X_t X_{t'}^\dagger \rangle_{t'}$, which contain products of dot operators and photon operators. If we are interested in small coupling parameters here, a decoupling of the reduced density matrix $\tilde{\rho}(t')$ can be written as

$$\tilde{\rho}(t') \approx \rho_{ph}^0 Tr_{ph} \tilde{\rho}(t'). \quad (3.16)$$

By using above equation, we obtain

$$Tr(\tilde{\rho}(t') \hat{n}_U X_t X_{t'}^\dagger) \approx \langle \hat{n}_U \rangle_{t'} \langle X_t X_{t'}^\dagger \rangle_0 \quad (3.17)$$

and correspondingly the other products of operators can be obtained also. For spontaneous emission, the photon bath is assumed to be in equilibrium. The expectation value $\langle X_t X_{t'}^\dagger \rangle_0 \equiv C(t-t')$ is a function of the time interval only. We can now define the Laplace transformation for real z ,

$$\begin{aligned} C_\varepsilon(z) &\equiv \int_0^\infty dt e^{-zt} e^{i\varepsilon t} C(t) \\ n_U(z) &\equiv \int_0^\infty dt e^{-zt} \langle \hat{n}_U \rangle_t \quad \text{etc.}, \quad z > 0 \end{aligned} \quad (3.18)$$

and transform the whole equations of motion into z -space,

$$\begin{aligned} n_U(z) &= -i \frac{g}{z} (p(z) - p^*(z)) + 2 \frac{\Gamma_U}{z} (1/z - n_U(z) - n_D(z)) \\ n_D(z) &= \frac{g}{z} (p(z) - p^*(z)) - 2 \frac{\Gamma_D}{z} n_D(z) \\ p(z) &= -ig \{ n_U(z) C_\varepsilon(z) - n_D(z) C_{-\varepsilon}^*(z) \} - \Gamma_D p(z) C_\varepsilon(z) \\ p^*(z) &= ig \{ n_U(z) C_\varepsilon^*(z) - n_D(z) C_{-\varepsilon}(z) \} - \Gamma_D p^*(z) C_\varepsilon^*(z). \end{aligned} \quad (3.19)$$

These equations can then be solved algebraically. The tunnel current \hat{I} can be defined as the change of the occupation of \hat{n}_U and is given by $\hat{I} \equiv ig(\hat{p} - \hat{p}^\dagger)$, where we have set the electron charge $e = 1$ for convenience. The time dependence of the expectation value $\langle \hat{I} \rangle_t$ can be obtained by solving Eqs. (3.19) and performing the inverse Laplace transformation. For time $t \rightarrow \infty$, the result is

$$\begin{aligned} \langle \hat{I} \rangle_{t \rightarrow \infty} &= \frac{2g^2 \Gamma_U \Gamma_D B}{g^2 \Gamma_D B + [g^2 B + \Gamma_D + 2\gamma \Gamma_D^2 + (\gamma^2 + \Omega^2) \Gamma_D^3]} \\ B &= \gamma + (\gamma^2 + \Omega^2) \Gamma_D, \end{aligned} \quad (3.20)$$

where $g^2 \Omega$ and $g^2 \gamma$ are the exciton frequency shift and decay rate, respectively. The derivation of the current equation is closely analogous to the spontaneous emission

of phonons in double dots [46], in which the correlation functions $\langle X_t X_{t'}^\dagger \rangle_0$ is given by the electron-phonon interaction.

As can be seen from Eq. (3.20), the stationary current through the quantum dot depends strongly on the decay rate γ . The tunnel currents of a quantum dot inside a planar microcavity is numerically displayed in Fig. 5. In plotting the figure, the current is in terms of 100 pA, and the cavity length is in units of $\lambda_0/2$, where λ_0 is the wavelength of the emitted photon. Furthermore, the tunneling rates, Γ_U and Γ_D , are assumed to be equal to $0.2\gamma_0$ and γ_0 , respectively. Here, a value of $1/1.3\text{ns}$ for the free-space quantum dot decay rate γ_0 is used in our calculations [47]. Also, the planar microcavity has a Lorentzian broadening at each resonant modes (with broadening width equals to 1% of each resonant mode) [38]. As the cavity length is less than half of the wavelength of the emitted photon, the stationary current is inhibited. This is because the energy of the photon generated by the quantum dot is less than the cut-off frequency of the planar microcavity. Moreover, the current is increased whenever the cavity length is equal to multiple half wavelength of the emitted photon. It represents as the cavity length exceeds some multiple wavelength, it opens up another decay channel abruptly for the quantum dot exciton, and turns out that the current is increased. With the increasing of cavity length, the stationary current becomes less affected by the cavity and gradually approaches to free space limit.

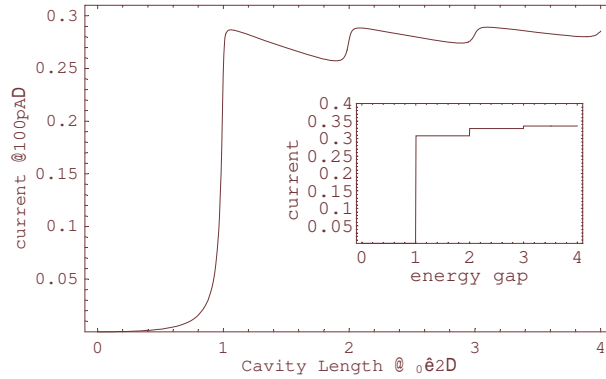


Figure 5: Stationary tunnel current, Eq. (3.20), as a function of cavity length L_c . The vertical and horizontal units are 100 pA and λ_0 , respectively. Inset : $\langle \hat{I} \rangle$ as a function of exciton energy gap ε . The cavity length is fixed to $\lambda_0/2$. The current is in units of 100 pA, while the energy gap is terms of $2hc/\lambda_0$.

To understand the inhibited current thoroughly, we now fix the cavity length equal to $\lambda_0/2$ and vary the exciton energy gap, while the planar microcavity is now assumed to be perfect. The vertical and horizontal units in the inset of Fig. 5 are 100 pA and $2hc/\lambda_0$, respectively. Here, λ_0 is the wavelength of the photon emitted by the quantum dot exciton in free space. Once again, we observe the suppressed

current as the exciton energy gap is tuned below the cut-off frequency. The plateau features in the inset of Fig. 5 also comes from the abruptly opened decay channels for the quantum dot exciton. From the experimental point of view, it is not possible to tune either the cavity length or the energy gap for such a wide range. A possible way is to vary the exciton gap around the first discontinuous point $2hc/\lambda_0$. Since the discontinuities should smear out for the real microcavity, it is likely to have a peak if one measures the differential conductance $d\langle I \rangle/d\varepsilon$ as a function of energy gap ε .

4 Current through the double-dot system and the induced entanglement

Now, we consider *two spatially separated* quantum dots incorporated inside the *p-i-n* junction. The novel feature here is the dissipative creation of entanglement over relatively large distances, and its readout via the stationary current. The device structure is shown in Fig. 6.

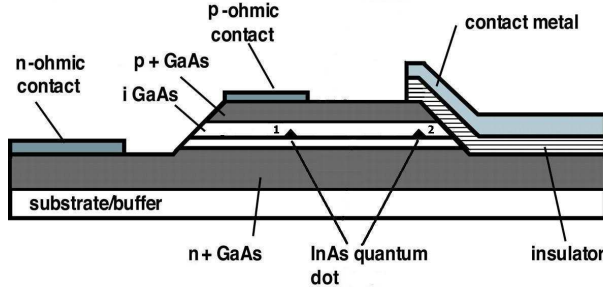


Figure 6: Proposed device structure. Two InAs quantum dots are embedded in a *p-i-n* junction. Above dot 2 is a metal gate, which control the energy gap and orientation of the dipole.

One of the obstacles in measuring superradiance between the quantum dots comes from the random size of the dots which result in a random distribution of energy gap and thus diminishes the coherent radiation. This can be overcome by constructing a gate voltage over one of the quantum dots. The energy gap and the orientation of the dipole moments of one of the quantum dots, thus can be controlled well.

After a hole is injected into the hole subband in the quantum dot, the *n*-side electron can tunnel into the exciton level because of the Coulomb interaction between the electron and hole. In our calculation, we also neglect the Forster process which may have some influences on the results if the two dots are close to each other. The validity of this assumption will be discussed later. Thus, we

may assume four dot states $|0\rangle = |0, h; 0, 0\rangle$, $|U_1\rangle = |e, h; 0, 0\rangle$, $|U_2\rangle = |0, 0; e, h\rangle$, and $|D\rangle = |0, 0; 0, 0\rangle$, where $|0, h; 0, 0\rangle$ means there is one hole in dot 1 and $|0, 0; 0, 0\rangle$ represents the ground state with no hole and electron in the quantum dots. The exciton states $|e, h; 0, 0\rangle$ (in dot 1) can be converted to $|0, 0; e, h\rangle$ (in dot 2) through the exciton-photon interactions. By transforming $|U_1\rangle$ and $|U_2\rangle$ into Dicke states: $|S_0\rangle = \frac{1}{\sqrt{2}}(|U_1\rangle - |U_2\rangle)$ and $|T_0\rangle = \frac{1}{\sqrt{2}}(|U_1\rangle + |U_2\rangle)$, we can now define the dot-operators $\hat{n}_S \equiv |S_0\rangle\langle S_0|$, $\hat{n}_T \equiv |T_0\rangle\langle T_0|$, $\hat{n}_D \equiv |D\rangle\langle D|$, $\hat{p}_s \equiv |S_0\rangle\langle D|$, $\hat{p}_T \equiv |T_0\rangle\langle D|$, $\hat{s}_{U_1} \equiv \frac{1}{\sqrt{2}}(|0\rangle\langle S_0| + |0\rangle\langle T_0|)$, $\hat{s}_D \equiv |0\rangle\langle D|$. The exciton-photon coupling is described by an interaction Hamiltonian H_T :

$$\begin{aligned} H_T &= \sum_{\mathbf{k}} \frac{1}{\sqrt{2}} g \{ D_{\mathbf{k}} b_{\mathbf{k}} [\hat{p}_S (1 + e^{i\mathbf{k}\cdot\mathbf{r}}) \\ &\quad + \hat{p}_T (1 - e^{i\mathbf{k}\cdot\mathbf{r}})] + c.c. \} \\ &= g (\hat{p}_S X_S + \hat{p}_S^\dagger X_S^\dagger + \hat{p}_T \overline{X}_T + \hat{p}_T^\dagger \overline{X}_T^\dagger), \end{aligned} \quad (4.1)$$

where \mathbf{r} is the position vector between two quantum dot, $X_S = \sum_{\mathbf{k}} (1 + e^{i\mathbf{k}\cdot\mathbf{r}}) D_{\mathbf{k}} b_{\mathbf{k}}$, and $\overline{X}_T = \sum_{\mathbf{k}} (1 - e^{i\mathbf{k}\cdot\mathbf{r}}) D_{\mathbf{k}} b_{\mathbf{k}}$. The dipole approximation is not used in our calculation since we keep the full $e^{i\mathbf{k}\cdot\mathbf{r}}$ terms in the operators X_S and \overline{X}_T . Following the derivations in previous section, one can also derive a master equation for this double dot system. The equations of motion can be expressed as

$$\begin{aligned} \langle \hat{n}_\sigma \rangle_t - \langle \hat{n}_\sigma \rangle_0 &= -ig \int_0^t dt' \{ \langle \hat{p}_\sigma \rangle_{t'} - \langle \hat{p}_\sigma^\dagger \rangle_{t'} \} \\ &\quad + \Gamma_U \int_0^t dt' (1 - \langle \hat{n}_S \rangle_{t'} - \langle \hat{n}_T \rangle_{t'} - \langle \hat{n}_D \rangle_{t'}) \\ \langle \hat{n}_D \rangle_t - \langle \hat{n}_D \rangle_0 &= -ig \int_0^t dt' \{ \langle \hat{p}_S \rangle_{t'} - \langle \hat{p}_S^\dagger \rangle_{t'} + \langle \hat{p}_T \rangle_{t'} - \langle \hat{p}_T^\dagger \rangle_{t'} \} \\ &\quad - 2\Gamma_D \int_0^t dt' \langle \hat{n}_D \rangle_{t'} \\ \langle \hat{p}_S \rangle_t - \langle \hat{p}_S \rangle_0^0 &= -\Gamma_D \int_0^t dt' e^{i\varepsilon(t-t')} \langle X_t X_{t'}^\dagger \widetilde{p}_S(t') \rangle_{t'} \\ &\quad - ig \int_0^t dt' e^{i\varepsilon(t-t')} \{ \langle \hat{n}_S X_t X_{t'}^\dagger \rangle_{t'} - \langle \hat{n}_D X_{t'}^\dagger X_t \rangle_{t'} \} \\ \langle \hat{p}_T \rangle_t - \langle \hat{p}_T \rangle_0^0 &= -\Gamma_D \int_0^t dt' e^{i\varepsilon(t-t')} \langle \overline{X}_t \overline{X}_{t'}^\dagger \widetilde{p}_T(t') \rangle_{t'} \\ &\quad - ig \int_0^t dt' e^{i\varepsilon(t-t')} \{ \langle \hat{n}_T \overline{X}_t \overline{X}_{t'}^\dagger \rangle_{t'} - \langle \hat{n}_D \overline{X}_{t'}^\dagger \overline{X}_t \rangle_{t'} \}, \end{aligned} \quad (4.2)$$

where the index $\sigma = S$ or T .

Similarly, the tunnel current \hat{I} can be defined as the change of the occupation of \hat{n}_D and is given by $\hat{I} \equiv ig \sum_{\sigma} (\hat{p}_{\sigma} - \hat{p}_{\sigma}^{\dagger})$. The expectation value $\langle \hat{I} \rangle_t$ can be obtained in the limit of $t \rightarrow \infty$ and reads

$$\langle \hat{I} \rangle_{t \rightarrow \infty} = \frac{4g^2\gamma_+\gamma_-}{\gamma_- + \gamma_+[1 + 2\gamma_-(g^2/\Gamma_D + g^2/\Gamma_U + \Gamma_D)]}, \quad (4.3)$$

where $g^2\gamma_+$ and $g^2\gamma_-$ are the superradiant and subradiant decay rate of the exciton, respectively.

The corresponding decay rate for superradiant and the subradiant channels is given by

$$g^2\gamma_{\pm} = \gamma_0 \left(1 \pm \frac{\sin(2\pi d/\lambda_0)}{2\pi d/\lambda_0}\right), \quad (4.4)$$

where d is the inter-dot distance and γ_0 is the exciton decay rate in a quantum dot. To display the dependence of the stationary current through the quantum dot on the dot distance d , we present the results of two identical quantum dots in Fig. 7. As

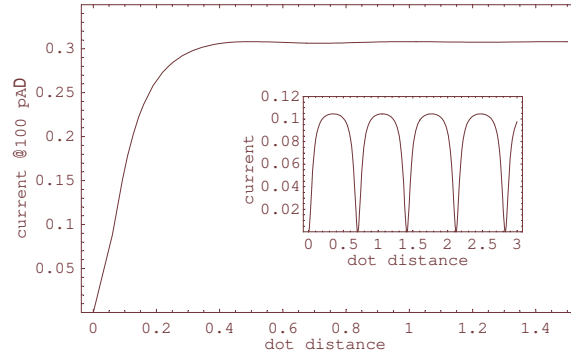


Figure 7: Stationary tunnel current as a function of dot distance d . The interference effect is seen clearly (inset) by incorporating the system inside a rectangular microcavity. The vertical and horizontal units are 100 pA and λ_0 , respectively.

shown in Fig. 7, the current is suppressed as the dot distance d is much smaller than the wavelength (λ_0) of the emitted photon. This corresponds to the trapping state in the two-ion system. As long as we choose only one of the dots to be coupled to reservoirs, the generated photon is reabsorbed immediately by the other dot and vice versa. The current is then blocked by this exchange process. For small rates limit ($g^2\gamma_{\pm}$) one can approximate Eq. (4.3) by $I \approx 4[1/g^2\gamma_- + 1/g^2\gamma_+]^{-1}$. The rates $\Gamma_{U,D}$ drop out completely and the current is only determined by the (smaller) radiative decay rates. In this approximate form, the current looks identical to the expression for the conductance $G \propto [1/\Gamma_L + 1/\Gamma_R]^{-1}$ from a left lead through a single level

to a right lead with tunnel rates $\Gamma_{L,R}$. This implies that the superradiant and the subradiant channel are in series (and not in parallel) in this limit. This is because once the exciton is formed in dot 1, time evolution of this state is proportional to $e^{-g^2\gamma_+t} + e^{-g^2\gamma_-t}$ not $e^{-g^2(\gamma_++\gamma_-)t}$ [28]. It means the two decay channels in our system are not in parallel. For long time behavior $t \rightarrow \infty$ and $\gamma_+ \gg \gamma_-$, the function $e^{-g^2\gamma_+t} + e^{-g^2\gamma_-t}$ approaches the limit of $e^{-g^2\gamma_-t}$, which is identical to the same limit of the function $e^{-\frac{g^2\gamma_+\gamma_-}{\gamma_++\gamma_-}t}$ (in series).

Similar to the two-ion superradiance [42], the current also exhibits oscillatory behavior as a function of dot distance. To observe the interference effect clearly, one may incorporate the system inside a microcavity since semiconductor cavities with strong electron-photon coupling have been realized experimentally by, e.g., Gérard *et al.* [48]. Reduction of the allowed k -state is expected to increase the magnitude of the oscillation. For example, if the system is placed inside a rectangular microcavity with length λ_0 , the decay rate for the two channels can be worked out straightforwardly:

$$g^2\gamma_{cav,\pm} = \frac{\gamma_0}{\pi} \left| 1 \pm e^{i2\pi d/(\sqrt{2}\lambda_0)} \right|^2. \quad (4.5)$$

The stationary current is plotted in the inset of Fig. 7, where a perfect (lossless) cavity is assumed. As we mentioned above, the amplitude of oscillation is larger than that in free space. However, the oscillation period is not half of the wavelength, but $\lambda_0/\sqrt{2}$. This is because the interference term is only influenced by the wave vector in the unconfined direction. Excluding the contributions from fundamental cavity modes, the effective wave vector can be expressed as

$$k_{eff} = \sqrt{\left(\frac{2\pi}{\lambda_0}\right)^2 - 2 * \left(\frac{\pi}{\lambda_0}\right)^2} = \frac{k_0}{\sqrt{2}}. \quad (4.6)$$

The oscillation period of the decay rate and the current is therefore increased by a factor of $\sqrt{2}$.

In Fig. 8, we plot the expectation value of n_S (n_T) as a function of the dot distance. The maximum entangled state ($|S_0\rangle$) is reached as $d \ll \lambda_0$. This is remarkable as the steady state is independent of the initial state. The entanglement is induced by the cooperative decoherence in the system. In a recent paper by Schneider *et al.* [49], the authors consider the behavior of an ion trap with all ions driven simultaneously and coupled collectively to a heat bath. They also found that the steady state of the ion trap can exhibit quantum entanglement. However, the concurrence of their system is below the value of unity (maximum entanglement). On the contrary, in our system the maximum entangled state can be generated by tuning the band gap of dot 2 (linear stark effect), i.e. control the on/off of the superradiance. Another advantage of our scheme is shown in the inset of Fig. 8. If the double-dot system is incorporated inside a rectangular microcavity, the maximum entangled states repeat as a function of inter-dot distance. This means even for remote separation, the entanglement can still be achieved. The reason

can be attributed to that the creation of entanglement in our model is governed by the interaction with a common heat bath [50], while conventional creation of entanglement depends on the direct interaction between two subsystems[51]. When two dots are coupled to the common photon fields, the collective decay process drives the system into the entangled states. The novel feature of the effect predicted here is that entanglement in fact can be controlled electrically (without applying a laser field) and read out in the form of a transport property, i.e., the electron *current* (as a function of the dot distance or, alternatively, the cavity length).

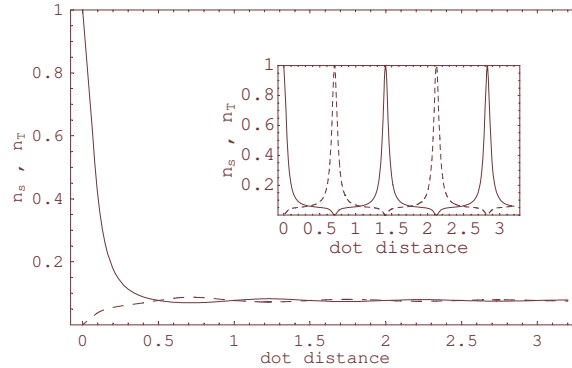


Figure 8: Occupation probability of the entangled states n_S (solid line) and n_T (dashed line). The inset shows the results inside a rectangular microcavity.

Another possible application of this effect is that by tuning the coherence of the dots, one can control the emission of single photon at predetermined times, which is important for the field of quantum information technology. One might argue that for small inter-dot distance the Forster process may play some role in our system[52]; nevertheless, this only causes small energy splitting between state $|S_0\rangle$ and $|T_0\rangle$. Comparing to the large energy difference in the III-V semiconductor material, its effect on the decay rate $g^2\gamma_{\pm}$ is negligible.

A few remarks about the problem of dissipation should be mentioned here. The coherence of the quantum states is a fundamental issue in quantum physics and decoherence caused by phonons or imperfections may destroy the unitary quantum evolution. In our proposals, decoherence due to interaction with other bosonic excitations (phonons and electron-hole pairs in the leads) is inevitable but can in principle be (partly) controlled by variation of the dot energies, or control of the mechanical degree of freedom[53]. In addition, scattering due to impurities are negligible since there is no interdot transport in our system.

5 Conclusions

In summary, we have proposed a new method of detecting superradiant and Purcell effects in semiconductor quantum dots. By incorporating a quantum dot between

a p-i-n junction, the Purcell effect on stationary tunnel current can be examined by the variations of cavity length or exciton gap. For the double-dot system, the superradiant effect on the stationary tunnel current can be examined by tuning the band gap of the quantum dot. The interference effects between two dots can be seen more clearly by incorporating the system inside a microcavity. The oscillation period of the decay rate and current is also increased because of the microcavity. Moreover, the maximum entangled state is induced as the inter-dot distance is much smaller than the wavelength of the emitted photon. Our model provides a new way to generate the entanglement in solid-state systems and maybe useful in future quantum information processing.

6 Acknowledgments

This work is supported partially by the National Science Council, Taiwan under the grant number NSC 93-2112-M-009-037.

References

- [1] R. H. Dicke, *Phys. Rev.* **93**, 99 (1954).
- [2] N. Skiribanowitz, I. P. Herman, J. C. MacGillivray, and M. S. Feld, *Phys. Rev. Lett.* **30**, 309 (1973).
- [3] M. Gross, C. Fabre, P. Pillet, and S. Haroche, *Phys. Rev. Lett.* **36**, 1035 (1976).
- [4] V. Ernst and P. Stehle, *Phys. Rev.* **176**, **1456** (1968).
- [5] Y. C. Lee and D. L. Lin, *Phys. Rev.* **183**, 147 (1969); **183**, 150 (1969).
- [6] F. Arechi and D. Kin, *Opt. Commun.* (Netherlands) **2**, **324** (1970).
- [7] J. J. Hopfield, *Phys. Rev.* **112**, 1555 (1958).
- [8] V. Agranovich and O. Dubovsky, *JETP Letters* **3**, 223 (1966).
- [9] K. C. Liu, Y. C. Lee, and Y. Shan, *Phys. Rev.* **B15**, 978 (1975).
- [10] K. C. Liu and Y. C. Lee, *Physica* **102A**, 131 (1980).
- [11] U. Cebulla, G. Bacher, A. Forchel, G. Mayer, and W. T. Tsang, *Phys. Rev. B* **39**, 6257 (1989).
- [12] B. Deveaud, F. Clerot, N. Roy, K. Satzke, B. Sermage, D. S. Katzer, *Phys. Rev. Lett* **67**, 2355 (1991).
- [13] E. Hanamura, *Phys. Rev.* **B 38**, 1228 (1988).

- [14] J. Knoester, *Phys. Rev. Lett.* **68**, 654 (1992).
- [15] D. S. Citrin, *Phys. Rev.* **B 47**, 3832 (1993).
- [16] G. Björk, Stanely Pau, Joseph M. Jacobson, Hui Cao, and Yoshihisa Yamamoto, *Phys. Rev.* **B 52**, 17310 (1995).
- [17] V. M. Agranovich, D. M. Basko, and O. A. Dubovsky, *J. Chem. Phys.* **106**, 3896 (1997).
- [18] Ya. Aaviksoo, Ya. Lippmaa, and T. Reinot, *Optics and Spectroscopy (USSR)* **62**, 419 (1987).
- [19] S. de Boer and D. A. Wiersma, *Chem. Phys. Lett.* **165**, 45 (1990).
- [20] J. Grad, G. Hernandez, and S. Mukamel, *Phys. Rev.* **A 37**, 3835 (1988).
- [21] A. L. Ivanov and H. Haug, *Phys. Rev. Lett.* **71**, 3182 (1993).
- [22] Y. Manabe, T. Tokihiro, and E. Hanamura, *Phys. Rev.* **B 48**, 2773 (1993).
- [23] A. Nakamura, H. Yamada, and T. Tookizaki, *Phys. Rev.* **B 40**, 8585 (1989).
- [24] T. Itch, M. Furumiya, and T. Ikehara, *Solid. State Comm.* **73**, 271 (1990).
- [25] F. C. Spano, J. R. Kuklinski, and S. Mukamel, *Phys. Rev. Lett.* **65**, 211 (1990).
- [26] O. A. Duboskii, *Phys. Solid State* **40**, 1937 (1998).
- [27] Y. C. Lee, D. S. Chuu, and W. N. Mei, *Phys. Rev. Lett.* **69**, 1081 (1992).
- [28] Y. C. Lee and D. L. Lin, *Phys. Rev.* **A 6**, 388 (1972).
- [29] Y. N. Chen and D. S. Chuu, *Phys. Rev.* **B 61**, 10815 (2000).
- [30] E. M. Purcell, *Phys. Rev.* **69**, 681 (1946).
- [31] J. Tignon, P. Voisin, C. Delalande, M. Voos, R. Houdre, U. Oesterle, and R. P. Stanley, *Phys. Rev. Lett.* **74**, 3967 (1995).
- [32] A. I. Tartakovskii, V. D. Kulakovskii, A. Forchel, and J. P. Reithmaier, *Phys. Rev.* **B 57**, R6807 (1998).
- [33] J. Bloch, R. Planel, V. Thierry-Mieg, J. M. Gérard, D. Barrier, J. Y. Marzin, and E. Costard, *Superlattice and Microstructure* **22**, 371 (1997).
- [34] G. S. Solomon, M. Pelton, and Y. Yamamoto, *Phys. Rev. Lett.* **86**, 3903 (2001).
- [35] C. Constantin, E. Martinet, A. Rudra, and E. Kapon, *Phys. Rev.* **B 59**, R7809 (1999).

- [36] A. V. Kavokin, M. A. Kaliteevski, and M. R. Vladimirova, *Phys. Rev. B* **54**, 1490 (1996).
- [37] A. V. Kavokin, E. L. Ivchenko, M. R. Vladimirova, M. A. Kaliteevski, and S. V. Goupalov, *Superlattice and Microstructure* **23**, 389 (1998).
- [38] Yueh-Nan Chen, Der-San Chuu, T. Brandes, and B. Kramer, *Phys. Rev. B* **64**, 125307 (2001).
- [39] A. Einstein, *Phys. Z.* **18**, 121 (1917).
- [40] V. Weisskopf and E. Wigner, *Z. Phys.* **63**, 54 (1930).
- [41] J. J. Sakurai, *Advanced Quantum Mechanics* (Addison-Wesley, Reading, Mass., 1967).
- [42] R. G. DeVoe and R. G. Brewer, *Phys. Rev. Lett.* **76**, 2049 (1996).
- [43] R. A. Römer and M. E. Raikh, *Phys. Rev. B* **62**, 7045 (2000).
- [44] O. Benson, C. Santori, M. Pelton, and Y. Yamamoto, *Phys. Rev. Lett.* **84**, 2513 (2001).
- [45] Z. Yuan, B. E. Kardynal, R. M. Stevenson, A. J. Shields, C. J. Lobo, K. Cooper, N. S. Beattie, D. A. Ritchie, M. Pepper, *Science* **295**, 102 (2002).
- [46] T. Brandes and B. Kramer, *Phys. Rev. Lett.* **83**, 3021 (1999).
- [47] G. S. Solomon, M. Pelton, and Y. Yamamoto, *Phys. Rev. Lett.* **86**, 3903 (2001).
- [48] J. M. Gerard *et al.*, *Phys. Rev. Lett.* **81**, 1110 (1998).
- [49] S. Schneider and G. J. Milburn, *Phys. Rev. A* **65**, 042107 (2002).
- [50] Y. N. Chen, D. S. Chuu, and T. Brandes, *Phys. Rev. Lett.* **16**, 166802 (2003).
- [51] Daniel Braun, *Phys. Rev. Lett.* **89**, 277901 (2002).
- [52] L. Quiroga and N. Johnson, *Phys. Rev. Lett.* **83**, 2270 (1999).
- [53] S. DeBald, T. Brandes, and B. Kramer, *Phys. Rev. B* **66**, 041301 (2002).